

# Disc Tearing and Bardeen-Petterson Alignment in GRMHD Simulations of Highly Tilted Thin Accretion Discs

M. Liska<sup>1\*</sup>, C. Hesp<sup>1,4,5</sup>, A. Tchekhovskoy<sup>2</sup>, A. Ingram<sup>3</sup>, M. van der Klis<sup>1</sup>, S.B. Markoff<sup>1</sup> & M. Van Moer<sup>6</sup>

<sup>1</sup>*Anton Pannekoek Institute for Astronomy, University of Amsterdam, Science Park 904, 1098 XH Amsterdam, The Netherlands*

<sup>2</sup>*Center for Interdisciplinary Exploration & Research in Astrophysics (CIERA), Physics & Astronomy, Northwestern University, Evanston, IL 60202, USA*

<sup>3</sup>*Department of Physics, Astrophysics, University of Oxford, Denys Wilkinson Building, Keble Road, Oxford, OX1 3RH, UK*

<sup>4</sup>*Amsterdam Brain and Cognition (ABC) Center, University of Amsterdam, Science Park 904, 1098 XH Amsterdam, The Netherlands*

<sup>5</sup>*Institute for Advanced Study (IAS), University of Amsterdam, Science Park 904, 1098 XH Amsterdam, The Netherlands*

<sup>6</sup>*National Center for Supercomputing Applications, University of Illinois at Urbana-Champaign, Urbana, IL 61801, USA*

Accepted. Received; in original form

## ABSTRACT

Luminous active galactic nuclei (AGN) and X-Ray binaries (XRBs) tend to be surrounded by geometrically thin, radiatively cooled accretion discs. According to both theory and observations, these are – in many cases – highly misaligned with the black hole spin axis. In this work we present the first general relativistic magnetohydrodynamic simulations of very thin ( $h/r \sim 0.015\text{--}0.05$ ) accretion discs around rapidly spinning ( $a \sim 0.9$ ) black holes and tilted by 45–65 degrees. We show that the inner regions of the discs with  $h/r \lesssim 0.03$  align with the black hole equator, though at smaller radii than predicted by theoretical work. The inner aligned and outer misaligned disc regions are separated by a sharp *break* in tilt angle accompanied by a sharp drop in density. We find that frame-dragging by the spinning black hole overpowers the disc viscosity, which is self-consistently produced by magnetized turbulence, *tearing* the disc apart and forming a rapidly precessing inner sub-disc surrounded by a slowly precessing outer sub-disc. We find that at all tilt values the system produces a pair of relativistic jets. At small distances the jets precess rapidly together with the inner sub-disc, whereas at large distances they partially align with the outer sub-disc and precess more slowly. If the tearing radius can be modeled accurately in future work, emission model independent measurements of black hole spin based on precession-driven quasi-periodic oscillations may become possible.

**Key words:** accretion, accretion discs – black hole physics – MHD – galaxies: jets – methods: numerical

## 1 INTRODUCTION

Because the gas supply of black holes (BHs) originates from far out, the angular momentum vector of the accreting gas tends to be independent of the BH spin vector. If the relative orientation of the two is random, the resulting accretion disc typically makes a 60-degree angle relative to the BH equator. Tilted discs are expected in many luminous systems ranging from X-ray binaries (XRBs), active galactic nuclei (AGN), tidal disruption events (TDEs), and binary merger remnant discs (e.g. Hjellming & Rupen 1995; Greene et al. 2001; Caproni et al. 2006, 2007; Abbott et al. 2017). The physics of tilted accretion systems is of crucial importance for understanding the growth of most – if not all – supermassive BHs

throughout cosmological time, and has profound implications for jet production, BH spin measurements, and energy release of BH accretion systems (e.g. Natarajan & Pringle 1998; Stella & Vietri 1998; Fiacconi et al. 2018).

Over time, tilted accretion discs get distorted by frame-dragging of their central BHs. The evolution of such warped discs depends sensitively on the ratio between their viscosity and aspect ratio (Papaloizou & Pringle 1983). The disc viscosity, parameterized through the  $\alpha$ -viscosity parameter, regulates the transport of angular momentum in the disc (Shakura & Sunyaev 1973). The disc aspect ratio,  $h/r$ , the ratio of disc scale height  $h$  to radius  $r$ , characterizes the internal pressure of the disc. When the disc is relatively thick,  $h/r > \alpha$ , such as in the hard state XRBs and low-luminosity AGN, the warps are transmitted by pressure waves traveling at about half the speed of sound (Papaloizou & Lin 1995).

\* matthewliska92@gmail.com

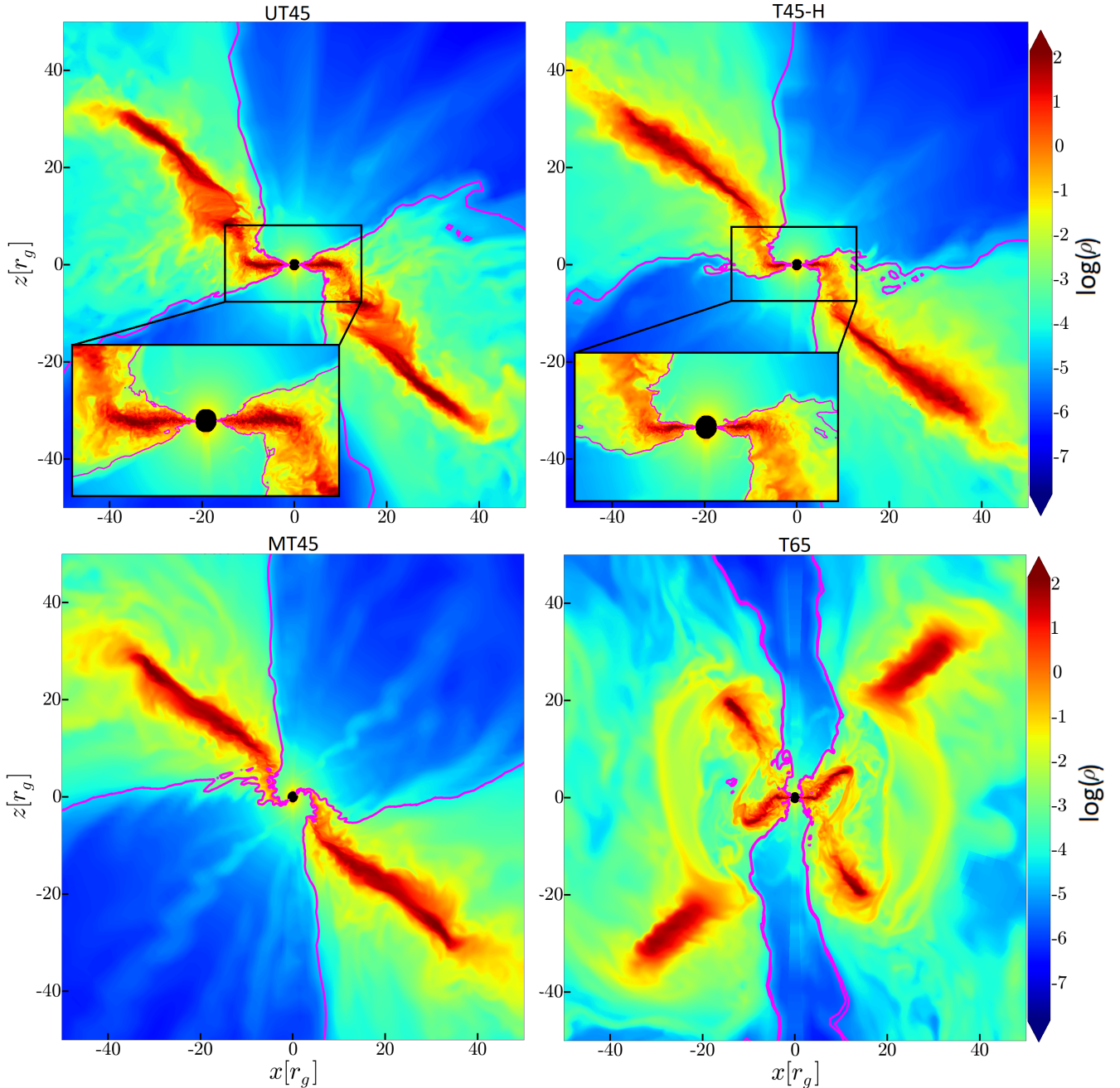


**Figure 1.** Clock-wise from top-left, panels show vertical slices through fluid frame density  $\log(\rho)$  for models UT45, T45-H at  $t = 7 \times 10^4 r_g/c$ , MT45 at  $t = 4.5 \times 10^4 r_g/c$  and T65 at  $t = 5.2 \times 10^4 r_g/c$  (red shows high and blue low values, see colour bar). Magenta lines indicate the jet boundary, defined as  $p_b = 5\rho c^2$ . All models except the thicker disc,  $h/r = 0.05$ , MT45 model, align with the BH spin. The Bardeen & Petterson (1975) alignment radius increases from  $r_{bp} \sim 5r_g$  in models T45, T65 and T45-H to  $r_{bp} \sim 10r_g$  in model UT45. The transition between aligned and misaligned disc regions is very sharp, forming a ‘break’ in tilt angle and density. In addition, the disc in model T65 forms a discontinuity in precession angle, tearing apart into multiple, differentially precessing, sub-discs (see also Fig. 3). Streamers transfer mass and angular momentum between sub-discs and directly to the BH.

In this wave-like limit, analytic calculations (Ivanov & Illarionov 1997; Lubow et al. 2002) and general-relativistic magnetohydrodynamic (GRMHD) simulations (Fragile et al. 2007; Morales Teixeira et al. 2014; Liska et al. 2018b, 2019a; White et al. 2019) have shown that the tilt of the disc oscillates as a function of radius within about 20 gravitational radii, such that material gets accreted at high inclination angles. When the disc is relatively thin,  $h/r < \alpha$ , warps are propagated through viscous diffusion, and radial tilt os-

cillations get damped by the dissipative effects of disc viscosity. This is the case in bright quasars and soft state X-ray binaries. In this limit, which is the focus of this work, a so-called *Bardeen-Petterson configuration* is expected to emerge: the inner disc aligns with the BH spin whereas the outer disc remains tilted (Bardeen & Petterson 1975). Since, by Newton’s third law, the torque exerted by the BH on the inner disc is exactly equal and opposite to the torque exerted by the inner disc on the BH, Bardeen & Petterson

(1975) alignment will not only align the disc with the BH spin, but will also torque the BH into alignment with the the outer disc (if the disc is massive enough). Thus, the Bardeen & Petterson (1975) effect substantially accelerates the alignment between disc and BH spin axes (because the specific angular momentum increases with radius), possibly leading to a rapid spin-up of supermassive BHs, even if discs during most accretion events are (initially) misaligned (e.g. Natarajan & Pringle 1998; King et al. 2005).

However, across both disc radius and height, there tend to be large, non-linear, and anisotropic variations of the viscous stresses induced by the magneto-rotational instability (MRI, Balbus & Hawley 1991; Balbus & Hawley 1998) in *magnetized* accretion discs, defying the simple  $\alpha$ -viscosity prescription (Penna et al. 2010; Sorathia et al. 2010; McKinney et al. 2012; Jiang et al. 2017). For example, recent GRMHD simulations (Liska et al. 2019b) of a very thin,  $h/r = 0.03$ , magnetized accretion disc tilted by  $10^\circ$  have shown that magnetic fields launch winds which counteract Bardeen & Petterson (1975) alignment in a strongly non-linear fashion, producing an aligned region that is much smaller than predicted for  $\alpha$ -discs (Kumar & Pringle 1985; Nelson & Papaloizou 2000; Lodato & Price 2010; Nixon & King 2012).

Crucially, when a thin  $\alpha$ -disc is tilted by  $\mathcal{T} \gtrsim 45^\circ$ , smoothed particle hydrodynamics (SPH) simulations suggest that frame-dragging by the spinning BH tears the disc apart into differentially precessing rings (Nixon et al. 2012b; Nealon et al. 2015). Just as in thin  $\alpha$ -discs, once a magnetized disc starts to tear, the viscosity may drop and encourage further tearing (Ogilvie 1999; Nixon & King 2012; Doğan et al. 2018). However, since the tilt (in radians) exceeds the disc’s scale height by more than an order in magnitude, the warp becomes highly non-linear – requiring a detailed treatment involving the 3D magnetized turbulence that is the glue that keeps the disc together. This is possible using GRMHD simulations, and in this paper we use them to study whether and how tilted, thin, magnetized discs can get torn apart. We pay special attention to the typical tearing radius and the physical prerequisites for tearing to occur. Forming such an understanding may pave the way for BH spin measurements based on quasi-periodic oscillations (QPOs) observed in XRB lightcurves (van der Klis 1989). Such QPOs could be driven by disc (Stella & Vietri 1998; Ingram et al. 2009, 2016) and/or jet (Kalamkar et al. 2016; Stevens & Uttley 2016) precession.

In this work we present the first GRMHD simulations of highly tilted thin accretion discs in the diffusive limit of warp propagation ( $h/r < \alpha$ ). In Section 2 we describe our code and initial conditions. We present our results in Sec. 3 and conclude in Sec. 4.

## 2 NUMERICAL METHOD AND INITIAL CONDITIONS

For this work we use our recently developed GRMHD code H-AMR (Liska et al. 2018b; Chatterjee et al. 2019; Porth et al. 2019). It evolves the GRMHD equations with a finite-volume-based method in modified Kerr-Schild coordinates (as in Gammie et al. 2003) and uses a constrained-transport scheme for magnetic field evolution (see Gardiner & Stone 2005). Here we employ a logarithmic spherical polar grid with 3 to 4 levels of adaptive mesh refinement (AMR) and 4 levels of local adaptive time-stepping, allowing us to focus the resolution on the regions of interest. In particular, magnetized turbulence in the disc needs to be resolved (Liska et al. 2018b), so we use rest-mass density  $\rho$  as the refinement criterion in order to delineate the disc (as in Liska et al. 2019b). In this way, we achieve the following effective resolutions in spher-

Model	Full name	$\mathcal{T}_{\text{init}}$	$N_r \times N_\theta \times N_\phi$	$h/r$	$t_i - t_f$ [ $10^4 t_g$ ]
T45	T45HR03L	$45^\circ$	$2880 \times 864 \times 1200$	0.03	0-10.5
T45-H	T45HR03H	$45^\circ$	$5760 \times 1728 \times 2400$	0.03	4.8-7.2
UT45	T45HR015H	$45^\circ$	$5760 \times 1728 \times 2400$	0.015	4.8-7.0
MT45	T45HR05L	$45^\circ$	$2880 \times 864 \times 1200$	0.05	0-4.5
T65	T65HR03L	$65^\circ$	$2880 \times 864 \times 1200$	0.03	0-12

**Table 1.** The tilt ( $\mathcal{T}_{\text{init}}$ ), number of cells in  $r$ -,  $\theta$ - and  $\phi$ - coordinates ( $N_r \times N_\theta \times N_\phi$ ), disc thickness ( $h/r$ ) and time interval ( $t_i - t_f$ ) for each model.

ical polar coordinates ( $N_r \times N_\theta \times N_\phi$ ):  $2880 \times 864 \times 1200$  in our low-resolution models, and, by doubling the resolution in every dimension,  $5760 \times 1728 \times 2400$  in our high resolution models (see Table 1). This resolves our thin discs by approximately 7 to 14 cells per scale height (see Sec. 3 for the MRI quality factors). We use out-flow boundary conditions at the inner and outer radial boundaries, which we place inside the event horizon and at  $10^5 r_g$ , respectively, where  $r_g = GM/c^2$  is the gravitational radius. This way both boundaries are causally disconnected from the accretion system. Across the polar singularity in  $\theta$  we use a transmissive boundary condition, which we implement using a multi-faceted method that minimizes numerical dissipation in the polar region (for details, see Liska et al. 2018b).

All models, shown in Table 1, are initially seeded with a Kerr black hole (with  $a = 0.9375$ ) surrounded by a torus in hydrostatic equilibrium (in accordance with Fishbone & Moncrief 1976) with its inner edge at  $r_{\text{in}} = 12.5 r_g$ , its pressure maximum at  $r_{\text{max}} = 25 r_g$ , and its density normalized by setting  $\max \rho = 1$ . We use the equation of state of an ideal gas,  $p_g = (\Gamma - 1) u_g$ , where  $p_g$  and  $u_g$  are thermal pressure and thermal energy density, and we use a polytropic index that corresponds to a non-relativistic monoatomic ideal gas,  $\Gamma = 5/3$ . We insert into the torus a poloidal magnetic field defined by a covariant vector potential  $A_\phi = (\rho - 0.05)^2 r^3$ . We normalize the magnetic field strength by requiring that  $\max p_g / \max p_b = 30$ , where  $p_b$  is the magnetic pressure. Subsequently, we tilt the torus and magnetic field relative to the BH spin (and the grid) by an angle  $\mathcal{T}_{\text{init}}$  (see Liska et al. 2018b for details). Finally, we reduce the disc thickness to a target scale-height  $h/r$  by cooling the gas at a rate slow enough to avoid disruption of the disc orbital dynamics. We do this by letting the internal energy decay exponentially over time, with the time constant set by the orbital timescale (Noble et al. 2009). Since the disc needs some time to cool and reach the target scaleheight, we only include data after  $t = 10^4 r_g/c$  into our analysis. We initialize the high-resolution models T45-H and UT45 with a well-evolved state of model T45 at  $t = 4.8 \times 10^4 t_g$ , where  $t_g = r_g/c$  (see Table 1 for details). In the case of T45-H, we, additionally, change the target thickness in the cooling function from  $h/r = 0.03$  to  $h/r = 0.015$ .

## 3 RESULTS

Figure 1 shows a colour map of the density for models UT45, T45-H, MT45 and T65 in their evolved state at  $t \gtrsim 4 \times 10^4 r_g/c$ . As can be seen from 3D animations (see this [YouTube playlist](#)), the inner disc always aligns with the BH spin in models T45-H and UT45, aligns most of the time in model T45, some of the time in model T65, and does not align at all in model MT45. This makes sense, since in model MT45 the disc is thicker,  $h/r = 0.05$ , and may fall outside the diffusive warp propagation regime,  $h/r < \alpha$ , where the Bardeen & Petterson (1975) alignment is expected (e.g. Ivanov & Illarionov 1997).

For our thinnest discs, we can establish the dependence of disc



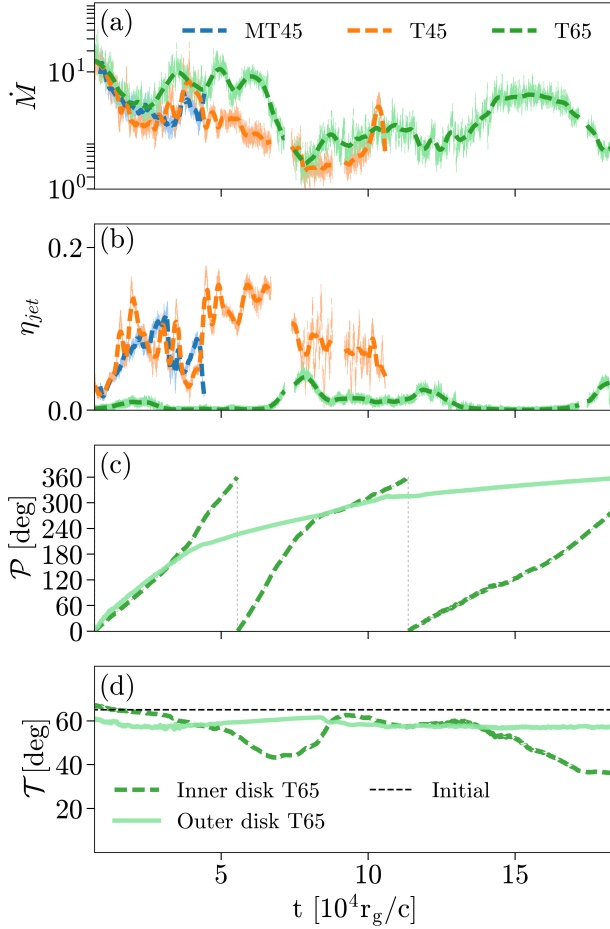


**Figure 2.** Time evolution for models T65 (green), T45 (orange) and MT45 (blue). [panel (a)] The BH mass accretion ( $\dot{M}_{BH}$ ) is about 1.5–3 times higher in T65 compared to the other two models, presumably due to cancellation of angular momentum when the sub-discs become partially opposed (Fig. 3). [panel (b)] The jet efficiency ( $\eta_{jet}$ , measured at  $r \sim 10r_g$ ) is reduced significantly in T65 due to dissipation when the jet gets reoriented at the tearing radius of  $r \sim 5 - 30r_g$ . [panel (c)] The precession angle ( $\mathcal{P}$ ) in T65 of the inner sub-disc (dotted) increases much more rapidly than the precession angle of the outer sub-disc (solid) due to the differential nature of the [Lense & Thirring \(1918\)](#) torque. [panel (d)] The inner sub-disc quickly starts aligning with the BH spin (i.e., decreasing  $\mathcal{T}$ ) during phases of disc tearing when there is a large difference in  $\mathcal{P}$  between the inner and outer sub-discs (e.g., between  $5-7.5 \times 10^4 t_g$ ). After the inner sub-disc makes a full cycle in  $\mathcal{P}$ , it conjoins again with the outer sub-disc and is torqued back into a tilted configuration.

structure on thickness. In particular, we observe that the [Bardeen & Petterson \(1975\)](#) alignment radius,  $r_{bp}$ , increases from  $r_{bp} \sim 5r_g$  at  $h/r = 0.03$  to  $r_{bp} \sim 10r_g$  at  $h/r = 0.015$ . While this is consistent with the predicted analytic scaling of  $r_{bp} \sim (h/r)^{-8/7}$  (e.g. [Kumar & Pringle 1985](#)), the proportionality constant for our simulation is much smaller than in the analytic scaling. This discrepancy might be due to the torques applied on the disc by the large-scale magnetically-powered disc outflows that counteract the [Bardeen & Petterson \(1975\)](#) alignment and reduce the value of  $r_{bp}$  ([Liska et al. 2019b](#)).

More generally, the [Bardeen & Petterson \(1975\)](#) alignment is variable in time: as seen from the movies, as a general trend, an

increase/decrease in BH mass accretion rate  $\dot{M}_{BH}$  (Fig. 2a) tends to accompany the periods of misalignment/alignment of the inner disc with the BH in models T45 and T65. This might be due to rapid accretion giving the disc insufficient time to align with the BH spin axis ([Liska et al. 2019b](#)).

We note that there are important qualitative differences in the simulation results presented here and our previous work, which considered a disc with exactly the same initial conditions but tilted by a much smaller angle ([Liska et al. 2019b](#)). For a value of tilt,  $\mathcal{T} = 10^\circ$ , the inner aligned and outer misaligned parts of the accretion disc were separated by a smooth warp ([Liska et al. 2019b](#)). However, for much larger tilt angles considered here,  $\mathcal{T} = 45-65$  degrees, the inner aligned and outer misaligned parts of the disc are separated by a discontinuity in tilt angle and sharp drop in density. This transition is referred to as a *disc break* (e.g., [Lodato & Price 2010; Nixon & King 2012](#)). As we discuss in Sec. 4, the development of a break may change the physical properties and observational signatures of a tilted disc and its precession.

Figures 1 and 3 show that at large values of tilt,  $\mathcal{T} = 65^\circ$ , in model T65, the disc tears into 2 or sometimes even 3 differentially precessing sub-discs at radii ranging from  $5r_g$  to  $30r_g$ . This is caused by the differential [Lense & Thirring \(1918\)](#) torques exceeding the viscous torques that keep the disc together. We observe that the disc also tears at lower tilt values,  $\mathcal{T} = 45^\circ$ , in models T45 and UT45: however, this happens at later times,  $t \gtrsim 10^5 r_g/c$  for T45 and  $t \gtrsim 7 \times 10^4 r_g/c$  for UT45. To get to the BH, the gas now accretes between sub-discs through streamers, which are tentacle-like low density structures connecting adjacent sub-discs, as seen in Figs 1 and 3. Note that the BP-aligned part of the inner sub-disc in Fig 1 is fed directly from the middle sub-disc, bypassing the misaligned part of the inner sub-disc.

As the phase difference in precession angle  $\mathcal{P}$  between the inner and outer sub-disc(s) builds up (Fig. 2c), this contributes to effective cancellation of angular momentum between the two ([Nixon et al. 2012a,b](#)). This might explain a factor of 1.5–3 enhancements in BH mass accretion rate (Fig. 2a) at  $t \sim 5 \times 10^4 r_g/c$  and  $t \sim 15 \times 10^4 r_g/c$  in model T65, corresponding to the moments in time when  $\mathcal{P}_{inner} - \mathcal{P}_{outer} = 180 + 360n$ ,  $n = 0, 1$  degrees, i.e., when the sub-discs are counter-rotating. Interestingly, the evolution of a sub-disc of radius  $10r_g$  formed at  $t \sim 4.5 \times 10^4 r_g/c$  differs from that of radius  $20 - 30r_g$  present throughout the simulation. While the smaller sub-disc slowly accretes into the BH, the large sub-disc temporarily merges with the outer sub-disc around  $t \sim 8 \times 10^4 r_g/c$  for a duration of  $t \sim 3.0 \times 10^4 r_g/c$  (both in precession angle  $\mathcal{P}$  and tilt angle  $\mathcal{T}$ , see Fig. 2c,d) before tearing again, but this time at a slightly larger radius of  $r \sim 30r_g$ . This merging may be driven by density fluctuations in the inner disc. Namely, during each precession cycle a significant portion of the inner disc mass falls into the BH (viscous timescale of inner disc equals  $\sim 1-3 \times 10^4 r_g/c$ ), which reduces the differential [Lense & Thirring \(1918\)](#) torque between inner and outer disc, allowing them to merge and subsequently tear at a different radius.

To gain a better insight into the internal disc dynamics in models UT45 and T65 we analyze radial profiles of density, plasma  $\beta = p_g/p_B$  and  $\alpha$ -viscosity, as shown in Fig. 4(a)-(d). Here, all vectors are calculated in a frame  $(r, \tilde{\theta}, \tilde{\phi})$  aligned with the rotation axis of the disc (see [Liska et al. 2019b](#) for details). Since  $\beta \gtrsim 1$  for  $r > 10r_g$  the disc remains (mostly) gas pressure dominated, except where the disc breaks or tears and the density drops. As expected for gas pressure dominated discs, we verified that the density weighted scale height,  $(h/r)_\rho = \langle \tilde{\theta} - \langle \tilde{\theta} \rangle_\rho \rangle_\rho$ , matches the thermal scale height,  $(h/r)_{thermal} = \langle c_s \rangle_\rho / \langle v_k \rangle_\rho$ , where  $v_k$  is the

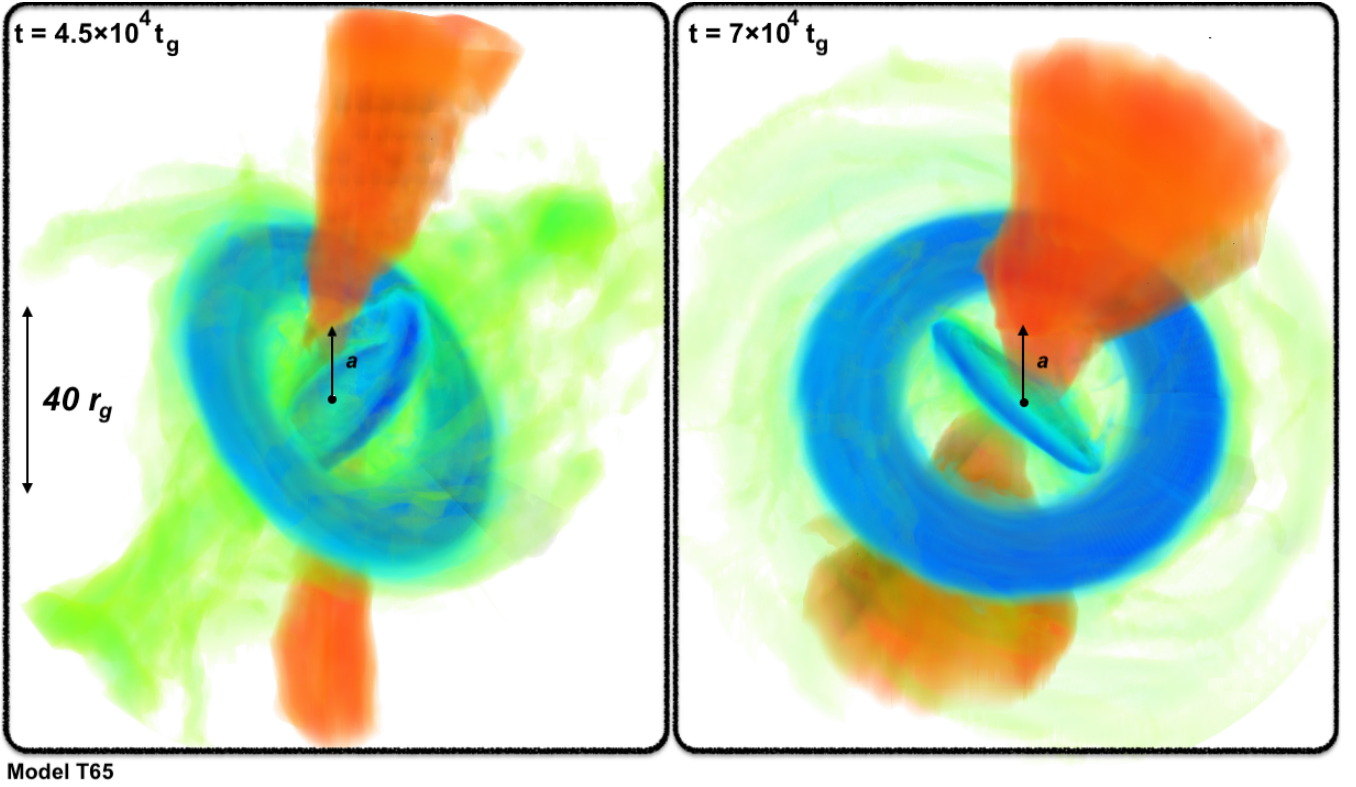


**Figure 3.** First demonstration that a highly tilted magnetized accretion disc (blue) can tear up into multiple, radially extended, sub-discs. In this volume rendering of model T65 at  $t = 4.5 \times 10^4 r_g/c$  (left) and  $t = 7 \times 10^4 r_g/c$  (right) the BH spin  $a$  is oriented vertically (black arrows) and the length scale of  $40 r_g$  is indicated on the left. The jet (red) is launched along the direction of the inner sub-disc, but, as it propagates outwards, tends to align with the corona (green), which is aligned with the outer sub-disc. While changing orientation, the jet exerts an equal and opposite force on the outer sub-disc, pushing it into more energetic orbits.

Keplerian 3-velocity,  $c_s$  is the sound speed, and  $\langle \dots \rangle_q$  indicates an angle-average weighted by the quantity  $q$ . Throughout the disc the sum of the Maxwell,  $\alpha_M = b^r b^\phi / (p_g + p_b)$ , and Reynolds,  $\alpha_R = \rho u^r u^\phi / (p_g + p_b)$ , stress contributions to the viscosity parameter remains larger than the disc scale height. This confirms that this disc is in the  $h/r < \alpha$  diffusive warp propagation regime (Papaloizou & Pringle 1983). Here,  $b^\mu$  and  $u^\mu$  are the magnetic and velocity 4-vectors.

Surprisingly, the effective viscosity parameter,  $\alpha_{eff} = -v_r v_k / c_s^2$ , which is a measure of the radial inflow speed, exceeds the sum of  $\alpha_R$  and  $\alpha_M$  by more than an order of magnitude. This indicates that the angular momentum transport in turbulent discs cannot be described by stresses induced through a local  $\alpha$ -viscosity. Most likely, similar to our  $\mathcal{T} = 10^\circ$  disc model described in Liska et al. (2019b), large-scale magnetic torques contribute to this discrepancy by transporting angular momentum away from the mid-plane into the upper layers of the disc, where it is subsequently carried away in the form of disc driven winds. Since the discrepancy between the effective viscosity parameter and Reynolds plus Maxwell stresses by up to a factor of  $\sim$ few exceeds those in the  $\mathcal{T} = 10^\circ$  tilt disc model, tilt-related effects, such as spiral shocks aligned with the line of nodes (Fragile & Blaes 2008; White et al. 2019), could also contribute to this discrepancy. Additionally, in our model T65, the cancellation of angular momentum could cause an increase in  $\alpha_{eff}$  during episodes of large misalignment between adjacent sub-discs. Observationally, this large, above unity, effective viscosity in the inner disc may cause electrons and ions to de-

couple into a two-temperature plasma (Esin et al. 1997, see also Sec. 4), forming a rapidly precessing advection-dominated accretion flow that produces a hard spectrum (Narayan & Yi 1994).

To verify numerical convergence, we compared the radial profiles of our model T45 and model T45-H, carried out a twice as high resolution, and found a good level of agreement. In addition, the number of cells per MRI wavelength,  $Q_r \times Q_\theta \times Q_\phi$ , saturates around  $100 \times 100 \times 500$  for  $r \lesssim 20 r_g$  and  $10 \times 10 \times 150$  for  $r \gtrsim 20 r_g$  in our low resolution models, indicating that the MRI turbulence is well-resolved in the inner and reasonably well-resolved in the outer regions of the accretion disc (Sorathia et al. 2010; Shiokawa et al. 2012).

All our models launch moderately strong Blandford & Znajek (1977) jets, which we define as magnetically-dominated regions with  $p_b / \rho c^2 > 5$ . Figure 2(b) shows that their energy outflow efficiency, or power measured in units of accretion power  $\dot{M}_{BH} c^2$ , reaches  $\eta_{jet} \sim 1\% - 10\%$ . Interestingly, the jets appear to follow the orientation of the disc over a wide range of length scales. For instance, jets at small radii align with the inner disc, as seen in Figs 3 and 4(e-h). At larger radii, they get torqued via the corona, (roughly) defined as all gas not part of the jet and whose density is a factor  $10^3$  smaller than that in the disc (see also Liska et al. 2019a), into (partial) alignment with the outer disc. This is also seen in Fig. 3. In fact, in model T65, the disc-jet interaction can be so strong that the jets running into outer sub-disc can push it into higher orbits (see this YouTube playlist). This may deprive the BH of its mass supply and quench the accretion at times be-

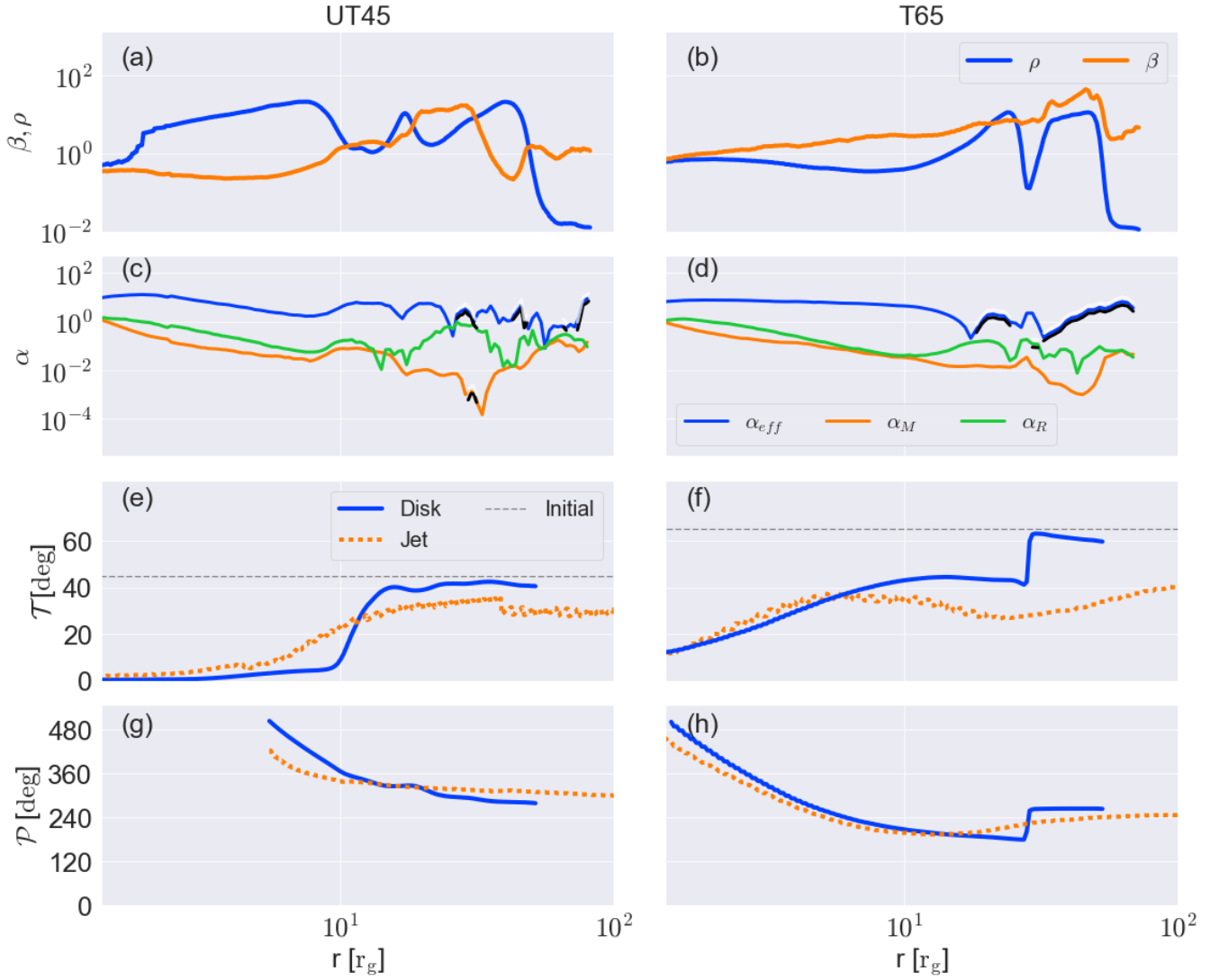


**Figure 4.** Radial profiles for models UT45 (left) and T65 (right) averaged over  $6.8 \times 10^4 r_g/c < t < 7.0 \times 10^4 r_g/c$ . [(a,b)] In both models the disc remains mostly gas-pressure dominated ( $\beta \gtrsim 1$ ) allowing it to achieve the target scale-height. The density ( $\rho$ ) drops around the disc breaking/tearing radius. [(c,d)] The effective viscosity ( $\alpha_{eff}$ ) exceeds the sum of the Maxwell ( $\alpha_M$ ) and Reynolds ( $\alpha_R$ ) stresses, presumably due to the presence of wind driven torques and, in T65, cancellation of angular momentum. Negative values of the effective viscosity ( $\alpha_{eff} \propto v_r$ ; black-white emphasis on the plots) are obtained when a particular annulus of the disc has net local outward movement (due to angular momentum transport). [(e-h)] The disc's and jet's tilt ( $\mathcal{T}$ ) and precession ( $\mathcal{P}$ ) angles tend to follow the same trend, since the outer disc torques the jet into (partial) alignment with itself. The discontinuity in tilt angle between inner and outer sub-disc in T65 occurs due to the angular momentum cancellation when the inner and outer sub-disc are partially opposed due to differential precession. It is unrelated to Bardeen & Petterson (1975) alignment.

yond those simulated. In nature, the outermost sub-disc would be essentially infinite in size, definitely much larger than in our simulations, and would have an essentially infinite precession period (Liska et al. 2018b). Due to the lack of precession of the outermost sub-disc, all precessing sub-discs would be located at smaller radii. Thus, only the parts of the jet outside of the aligned region,  $r \gtrsim r_{bp}$ , and inside of the outermost, non-precessing sub-disc would be expected to contribute to jet-driven QPOs (e.g., Kalamkar et al. 2016; Stevens & Uttley 2016).

#### 4 DISCUSSION AND CONCLUSION

In this work we have presented the first GRMHD simulations of highly tilted ( $\mathcal{T} = 45\text{--}65$  degrees), thin ( $h/r = 0.015\text{--}0.05$ ) accretion discs around rapidly spinning BHs ( $a = 0.9375$ ). We demonstrate for the first time that in the presence of realistic magnetized turbulence the inner parts of such discs can align with the BH spin axis, as predicted by Bardeen & Petterson (1975). However, we find that the alignment radius of  $r_{bp} \lesssim 5 - 10 r_g$  (Fig. 1) is much smaller than predicted by analytic models. This discrepancy may be caused by magnetically driven winds, which remove angular momentum from the inner disc, leading to a high radial infall speed and, thus, giving the inner disc insufficient time to align (see Liska et al. 2019b for discussion).



Since by Newton’s third law the torque exerted by the BH on the disc is equal and opposite to the torque exerted by the disc on the BH, the Bardeen & Petterson (1975) effect can torque the BH into alignment with the outer disc (if the disc’s angular momentum exceeds the BH’s angular momentum Natarajan & Pringle 1998; King et al. 2005; Fiacconi et al. 2018). The resulting aligned accretion can lead to rapid BH spinup to high spin. This can lead to powerful Blandford & Znajek (1977) jets in the presence of large scale poloidal or toroidal magnetic flux (e.g., Tchekhovskoy et al. 2011; McKinney et al. 2012; Liska et al. 2018a). Consistent with semi-analytic work (Nixon & King 2012) and smoothed-particle hydrodynamics (SPH) simulations (Lodato & Price 2010) the transition between the inner aligned and outer misaligned discs occurs over a very short distance and exhibits a sharp drop in density. As gas crosses this ‘break’, misaligned angular momentum cancels rapidly, possibly leading to enhanced dissipation of kinetic and magnetic energy causing non-thermal emission.

When the disc tilt is large,  $\mathcal{T} \gtrsim 45^\circ$ , we show for the first time that a magnetized thin  $h/r = 0.015$ – $0.03$  disc can tear into multiple independently precessing sub-discs, as seen in Fig. 3. In future work we will investigate whether tearing can happen at smaller values of disc tilt for thinner discs and whether, therefore, even weakly misaligned discs in XRBs and AGN can be subject to disc tearing. Observationally, we expect disc tearing to lead to a wide range of interesting phenomena. Differential precession, as explained in Sec. 3, can lead to cancellation of angular momentum leading to a factor of few increase in the mass accretion rate. This may explain flaring in the hard-intermediate/ultra-luminous state of XRBs (Remillard & McClintock 2006; McClintock & Remillard 2006). For instance if a disc undergoes several tearing events in quick succession, its luminosity will increase. However, the inner disc density eventually drops, because the outer disc is unable able to keep up the supply of gas indefinitely, especially when a powerful jet injects energy and angular momentum into the outer disc (Sec. 3). This drop in density, together with a very short accretion time (due to unusually large  $\alpha_{eff} \gtrsim 1$  in Fig. 4c,d), may lead to the decoupling of ions and electrons into a two-temperature plasma, reducing the ability of ions in the disc to cool and puffing up the inner thin disc into a hotter, and less radiatively efficient, thick advection-dominated accretion flow (ADAF, see Narayan & Yi 1994). In fact, for  $\alpha_{eff} > 1$  a thick disc would be expected to always form when two-temperature thermodynamics effects are taken into account (see e.g. Esin et al. 1997; Ferreira et al. 2006; Marcel et al. 2018a,b; Liska et al. 2019b). Since the viscous torque is stronger for a larger disc thickness, the thicker disc would no longer undergo tearing. For instance, our thicker disc model MT45 with  $h/r = 0.05$ , seen in the bottom-left panel of Fig. 1, does not show any signs of tearing. In its absence, the connection with the outer thin disc gets reestablished. The outer disc then feeds the inner one, and the BH mass accretion rate rises. This results in the density increase of the inner disc and its rapid cooling and collapse into a thin disc. The cycle then repeats. During each such cycle magnetic jets violently interact with the precessing sub-discs, making the tearing radius an interesting location for enhanced dissipation and (non-)thermal emission. Additionally, the streamers connecting torn sub-discs to each other can scatter and/or reradiate the emission from the central regions, substantially affecting the emergent spectrum and variability and making the discs appear larger than otherwise. This may resolve the puzzle of what makes AGN disc sizes exceed the predictions of an  $\alpha$ -disc model (e.g., Blackburne et al. 2011).

It has been suggested that BH spin could be measured based on precession induced Type-C QPOs (Stella & Vietri 1998; Ingram

et al. 2009), whose frequency depends on BH spin and disc size. Such measurements would be able to independently verify the accuracy of the continuum fitting (e.g. McClintock et al. 2014) and iron-line methods (e.g. Reynolds & Fabian 2008) without making any assumptions about the disc’s emission near the innermost stable circular orbit (ISCO) or assuming that the system is aligned. Making self-consistent predictions for the tearing radius, based on e.g. disc thickness, tilt and magnetic field topology, requires clear theoretical understanding of the physics driving disc tearing. On a basic level, for a disc to tear, the differential Lense & Thirring (1918) torques need to exceed the viscous torques holding the disc together. For  $\alpha$ -discs, the effective torque counteracting breaking and tearing can be derived as function of warp amplitude (Ogilvie 1999) making it possible to calculate criteria for disc breaking and tearing (Doğan et al. 2018). However, disc tearing in GRMHD leads to a substantially different morphology compared to SPH simulations (Nixon et al. 2012b; Nealon et al. 2015). More specifically, instead of tearing up into narrow ‘rings’ with  $\Delta r \sim h$  as seen in SPH models, our GRMHD models form radially extended sub-discs with  $\Delta r \gg h$  (Fig. 3). This suggests the disc tearing process may be more complicated when magnetized turbulence self-consistently determines the viscous-like coupling within the disc. We hypothesize that this might be caused by radial tension along magnetic field lines, which is neglected in the  $\alpha$ -disc approximation. These and other questions, such as how a disc break influences the angular momentum transport and what causes the apparent stochasticity in the disc tearing radius (see Sec. 3), will be addressed in future work.

## 5 ACKNOWLEDGMENTS

This research was made possible by NSF PRAC awards no. 1615281 and OAC-1811605 as part of the Blue Waters sustained-petascale computing project, which is supported by the National Science Foundation (awards OCI-0725070 and ACI-1238993) and the state of Illinois. Blue Waters is a joint effort of the University of Illinois at Urbana-Champaign and its National Center for Supercomputing Applications. ML and MK were supported by the NWO Spinoza Prize, AI by the Royal Society URF, CH by the NWO Research Talent grant (no. 406.18.535), SM by the NWO VICI grant (no. 639.043.513), and AT by the NSF grant 1815304 and NASA grant 80NSSC18K0565.

## 6 SUPPORTING INFORMATION

Additional Supporting Information may be found in the online version of this article: movie files. See our YouTube playlist for 3D visualizations of all models.

## REFERENCES

- Abbott B. P., et al., 2017, *Physical Review Letters*, 118, 221101
- Balbus S. A., Hawley J. F., 1991, *ApJ*, 376, 214
- Balbus S. A., Hawley J. F., 1998, *Rev. Mod. Phys.*, 70, 1
- Bardeen J. M., Petterson J. A., 1975, *ApJ*, 195, L65
- Blackburne J. A., Pooley D., Rappaport S., Schechter P. L., 2011, *ApJ*, 729, 34
- Blandford R. D., Znajek R. L., 1977, *MNRAS*, 179, 433
- Caproni A., Abraham Z., Mosquera Cuesta H. J., 2006, *ApJ*, 638, 120

- Caproni A., Abraham Z., Livio M., Mosquera Cuesta H. J., 2007, *MNRAS*, **379**, 135
- Chatterjee K., Liska M., Tchekhovskoy A. e., Markoff S. B., 2019, arXiv e-prints, p. [arXiv:1904.03243](#)
- Doğan S., Nixon C. J., King A. R., Pringle J. E., 2018, *MNRAS*, **476**, 1519
- Esin A. A., McClintock J. E., Narayan R., 1997, *ApJ*, **489**, 865
- Ferreira J., Petrucci P. O., Henri G., Saugé L., Pelletier G., 2006, *A&A*, **447**, 813
- Fiacconi D., Sijacki D., Pringle J. E., 2018, *MNRAS*, **477**, 3807
- Fishbone L. G., Moncrief V., 1976, *ApJ*, **207**, 962
- Fragile P. C., Blaes O. M., 2008, *ApJ*, **687**, 757
- Fragile P. C., Blaes O. M., Anninos P., Salmonson J. D., 2007, *ApJ*, **668**, 417
- Gammie C. F., McKinney J. C., Tóth G., 2003, *ApJ*, **589**, 444
- Gardiner T. A., Stone J. M., 2005, *Journal of Computational Physics*, **205**, 509
- Greene J., Bailyn C. D., Orosz J. A., 2001, *ApJ*, **554**, 1290
- Hjellming R. M., Rupen M. P., 1995, *Nature*, **375**, 464
- Ingram A., Done C., Fragile P. C., 2009, *MNRAS*, **397**, L101
- Ingram A., van der Klis M., Middleton M., Done C., Altamirano D., Heil L., Uttley P., Axelsson M., 2016, *MNRAS*, **461**, 1967
- Ivanov P. B., Illarionov A. F., 1997, *MNRAS*, **285**, 394
- Jiang Y.-F., Stone J., Davis S. W., 2017, preprint, ([arXiv:1709.02845](#))
- Kalamkar M., Casella P., Uttley P., O'Brien K., Russell D., Maccarone T., van der Klis M., Vincentelli F., 2016, *MNRAS*, **460**, 3284
- King A. R., Lubow S. H., Ogilvie G. I., Pringle J. E., 2005, *MNRAS*, **363**, 49
- Kumar S., Pringle J. E., 1985, *MNRAS*, **213**, 435
- Lense J., Thirring H., 1918, *Physikalische Zeitschrift*, **19**
- Liska M. T. P., Tchekhovskoy A., Quataert E., 2018a, arXiv e-prints,
- Liska M., Hesp C., Tchekhovskoy A., Ingram A., van der Klis M., Markoff S., 2018b, *MNRAS*, **474**, L81
- Liska M., Hesp C., Tchekhovskoy A., Ingram A., van der Klis M., Markoff S. B., 2019a, *MNRAS*, submitted ([arXiv:1901.05970](#)),
- Liska M., Tchekhovskoy A., Ingram A., van der Klis M., 2019b, *MNRAS*, accepted ([arXiv:1810.00883](#)), p. [arXiv:1810.00883](#)
- Lodato G., Price D. J., 2010, *MNRAS*, **405**, 1212
- Lubow S. H., Ogilvie G. I., Pringle J. E., 2002, *MNRAS*, **337**, 706
- Marcel G., et al., 2018a, *A&A*, **615**, A57
- Marcel G., et al., 2018b, *A&A*, **617**, A46
- McClintock J. E., Remillard R. A., 2006, Black hole binaries. pp 157–213
- McClintock J. E., Narayan R., Steiner J. F., 2014, *Space Sci. Rev.*, **183**, 295
- McKinney J. C., Tchekhovskoy A., Blandford R. D., 2012, *MNRAS*, **423**, 3083
- Morales Teixeira D., Fragile P. C., Zhuravlev V. V., Ivanov P. B., 2014, *ApJ*, **796**, 103
- Narayan R., Yi I., 1994, *ApJ*, **428**, L13
- Natarajan P., Pringle J. E., 1998, *ApJ*, **506**, L97
- Nealon R., Price D. J., Nixon C. J., 2015, *MNRAS*, **448**, 1526
- Nelson R. P., Papaloizou J. C. B., 2000, *MNRAS*, **315**, 570
- Nixon C. J., King A. R., 2012, *MNRAS*, **421**, 1201
- Nixon C. J., King A. R., Price D. J., 2012a, *MNRAS*, **422**, 2547
- Nixon C., King A., Price D., Frank J., 2012b, *ApJ*, **757**, L24
- Noble S. C., Krolik J. H., Hawley J. F., 2009, *ApJ*, **692**, 411
- Ogilvie G. I., 1999, *MNRAS*, **304**, 557
- Papaloizou J. C. B., Lin D. N. C., 1995, *ARA&A*, **33**, 505
- Papaloizou J. C. B., Pringle J. E., 1983, *MNRAS*, **202**, 1181
- Penna R. F., McKinney J. C., Narayan R., Tchekhovskoy A., Shafee R., McClintock J. E., 2010, *MNRAS*, **408**, 752
- Porth O., et al., 2019, arXiv e-prints, p. [arXiv:1904.04923](#)
- Remillard R. A., McClintock J. E., 2006, *ARA&A*, **44**, 49
- Reynolds C. S., Fabian A. C., 2008, *ApJ*, **675**, 1048
- Shakura N. I., Sunyaev R. A., 1973, *A&A*, **24**, 337
- Shiokawa H., Dolence J. C., Gammie C. F., Noble S. C., 2012, *ApJ*, **744**, 187
- Sorathia K. A., Reynolds C. S., Armitage P. J., 2010, *ApJ*, **712**, 1241
- Stella L., Vietri M., 1998, *ApJ*, **492**, L59
- Stevens A. L., Uttley P., 2016, *MNRAS*, **460**, 2796
- Tchekhovskoy A., Narayan R., McKinney J. C., 2011, *MNRAS*, **418**, L79
- White C. J., Quataert E., Blaes O., 2019, [arXiv:1902.09662](#),
- van der Klis M., 1989, *Annual Review of Astronomy and Astrophysics*, **27**, 517